social networks and collection of edible plant resources, may have encouraged regular descents to lower elevations.

Lithic tools and debitage of nonlocal fine-grained rocks, some with stream-polished cortex (Fig. 2C), suggest that Terminal Pleistocene and Early Holocene plateau residents ventured periodically to high-energy rivers below the plateau. Formal tools of Alca-4 obsidian at Cuncaicha originated in outcrops near the plateau edge ~22 km southwest (*21*) (Fig. 1B). Contemporary sites at Quebrada Jaguay on the Pacific Coast contain Alca-1, -4, and -5 obsidian tools and debitage (*9*, *23*); the only source of these three obsidians is the Pucuncho Basin and surrounding plateau (*21*). The oldest dates at Quebrada Jaguay and Cuncaicha overlap at two standard deviations. These sites likely constitute end members in a coast-highland Paleoindian settlement system.

Pleistocene glaciers did not present a barrier to human migration and settlement of the Pucuncho Basin. Glacial-geologic records from adjacent Nevado Coropuna (*32*) suggest that local glaciers reached their late-Pleistocene maxima ~25 to 20 ka and even then did not encroach into the basin. After a relatively minor readvance ~13.4 ka (*26*) (Fig. 3 and table S7), glaciers again receded. Southward displacement of the intertropical convergence zone ~13.0 to 11.5 ka (*33*) probably resulted in increased wet-season precipitation. The arrival of humans to the Pucuncho Basin coincided with a period of warming climate and enhanced primary productivity in plateau habitats.

Our data do not support previous hypotheses, which suggested that climatic amelioration and a lengthy period of human adaptation were necessary for successful human colonization of the high Andes. The Pucuncho Basin sites postdate the oldest known South American lowland site, Monte Verde (*13*), by only ~2 ky. Because early settlement of high-altitude regions is understudied, additional Terminal Pleistocene sites above 4000 masl likely await discovery. The Pucuncho Basin sites suggest that Pleistocene humans lived successfully at extreme high altitude, initiating organismal selection (*34*), developmental functional adaptations (*35*), and lasting biogeographic expansion in the Andes. As new studies (*36*–*38*) identify potential genetic signatures of high-altitude adaptation in modern Andean populations, comparative genomic, physiologic, and archaeological research will be needed to understand when and how these adaptations evolved.

REFERENCES AND NOTES

1. P. T. Baker, M. A. Little, *Man in the Andes: Multidisciplinary Study of High-Altitude Quechua* (Dowden, Hutchinson, and Ross, Stroudsberg, PA, 1976).
2. B. M. Marriot, S. J. Carlson-Newberry, Eds., *Nutritional Needs in Cold and High-Altitude Environments: Applications for Military Personnel in Field Operations* (National Academy Press, Washington, DC, 1996).
3. M. S. Aldenderfer, *World Archaeol.* **38**, 357–370 (2006).
4. All ages and ranges are two-sigma calibrated (2-σ cal).
5. P. J. Brantingham *et al.*, *Geoarchaeol.* **28**, 413–431 (2013).
6. K. Rademaker, G. R. M. Bromley, D. H. Sandweiss, *Quat. Int.* **301**, 34–45 (2013).
7. C. Méndez Melgar, *Quat. Int.* **301**, 60–73 (2013).
8. L. Prates, G. Politis, J. Steele, *Quat. Int.* **301**, 104–122 (2013).
9. D. H. Sandweiss *et al.*, *Science* **281**, 1830–1832 (1998).
10. S. deFrance, N. Grayson, K. Wise, *J. Field Archaeol.* **34**, 227–246 (2009).
11. D. Jackson, C. Méndez, R. Seguel, A. Maldonado, G. Vargas, *Curr. Anthropol.* **48**, 725–731 (2007).
12. T. D. Dillehay *et al.*, *Quat. Res.* **77**, 418–423 (2012).
13. T. D. Dillehay *et al.*, *Science* **320**, 784–786 (2008).
14. J. Steele, G. Politis, *J. Archaeol. Sci.* **36**, 419–429 (2009).
15. T. F. Lynch, *Guitarrero Cave: Early Man in the Andes* (Academic Press, New York, 1980).
16. E. A. Jolie, T. F. Lynch, P. R. Geib, J. M. Adovasio, *Curr. Anthropol.* **52**, 285–296 (2011).
17. M. Grosjean, L. Núñez, I. Cartajena, *J. Quat. Sci.* **20**, 643–653 (2005).
18. C. M. Santoro, L. Núñez, *Andean Past* **1**, 57–109 (1987).
19. Singular Terminal Pleistocene dates from Peruvian sites Pachamachay, Telarmachay, and PAn 12-58 are problematic (*6*) and generally rejected by the investigators; therefore, they are not included in this discussion.
20. J. W. Rick, K. M. Moore, *Boletín de Arqueología* **3**, 263–296 (1999).
21. K. Rademaker *et al.*, *Geology* **41**, 779–782 (2013).
22. K. Rademaker, D. A. Reid, G. R. M. Bromley, in *Least Cost Analysis of Social Landscapes: Archaeological Case Studies*. D. A. White, S. Surface-Evans, Eds. (University of Utah Press, Salt Lake City, UT, 2012), pp. 32–44.
23. K. Rademaker, thesis, University of Maine, Orono (2012).
24. U. Dornbusch, *Erdkunde* **52**, 41–54 (1998).
25. L. J. Jackson, in *Paleoindian Archaeology: A Hemispheric Perspective*. J. E. Morrow, C. Gnecco, Eds. (University of Florida Press, Gainesville, 2006), pp. 105–122.
26. Materials and methods are available as supporting materials on *Science* Online.
27. L. Perry *et al.*, *Nature* **440**, 76–79 (2006).
28. C. J. Klink, M. S. Aldenderfer, in *Advances in Titicaca Basin Archaeology, vol. 1.* C. Stanish, A. B. Cohen, M. S. Aldenderfer, Eds. (Cotsen Institute of Archaeology at UCLA, Los Angeles, 2005), pp. 25–54.
29. W. L. Franklin, in *Mammalian Biology in South America*, M. A. Mares, H. H. Genoways, Eds. (Volume 6, Special Publication Series, Pymatuning Laboratory of Ecology, University of Pittsburgh, Pittsburgh, 1981), pp. 457–489.
30. J. G. Hather, *Archaeological Parenchyma* (Archetype Publications, London, 2000).
31. J. W. Rick, *Prehistoric Hunters of the High Andes* (Academic Press, New York, 1980).
32. G. R. M. Bromley *et al.*, *Quat. Sci. Rev.* **28**, 2514–2526 (2009).
33. P.-H. Blard *et al.*, *Quat. Sci. Rev.* **30**, 3973–3989 (2011).
34. K. M. Weiss, A. W. Bigham, *Evol. Anthropol.* **16**, 164–171 (2007).
35. A. R. Frisancho, *Am. J. Hum. Biol.* **25**, 151–168 (2013).
36. A. W. Bigham *et al.*, *Am. J. Hum. Biol.* **25**, 190–197 (2013).
37. D. Zhou *et al.*, *Am. J. Hum. Genet.* **93**, 452–462 (2013).
38. C. A. Eichstaedt *et al.*, *PLOS ONE* **9**, e93314 (2014).
39. M. Stuiver, P. J. Reimer, *Radiocarbon* **35**, 215–230 (1993).
40. G. K. Ward, S. R. Wilson, *Archaeometry* **20**, 19–31 (1978).
41. A. G. Hogg *et al.*, *Radiocarbon* **55**, 1889–1903 (2013).

ACKNOWLEDGMENTS

Field work was supported by the Churchill Exploration Fund, National Geographic Society Waitt Foundation, Foundation for Exploration and Research on Cultural Origins, American Philosophical Society, and Lambda Alpha. B. Robinson and B. Hall funded pilot AMS dates. National Science Foundation Dissertation Grant no. 1208748 funded the AMS chronology. Pucuncho Basin pastoralists graciously allowed field work on their lands. A. Chu, R. Hintz, C. Mauricio, A. Ramos, A. Saenz, and E. Zuñiga provided invaluable logistical support. We thank field assistants W. Beckwith, K. Gardella, M. Koehler, T. Labanowski, O. McGlamery, E. Olson, and J. Wertheim and the staff of the Arizona AMS Laboratory. E. Cooper created Fig. 2. T. Koffman and P. Strand calibrated C-II ^{3}He ages for Fig. 3. Two anonymous reviewers provided helpful comments on the manuscript. Additional data are available in the supplementary materials. Artifact collections are curated at the Ministry of Culture in Arequipa, Peru.

SUPPLEMENTARY MATERIALS

www.sciencemag.org/content/346/6208/466/suppl/DC1
Materials and Methods
Figs. S1 to S6
Tables S1 to S7
References (*42*–*88*)

3 July 2014; accepted 16 September 2014
10.1126/science.1258260

PLANT SCIENCE

Antheridiogen determines sex in ferns via a spatiotemporally split gibberellin synthesis pathway

Junmu Tanaka,[1]* Kenji Yano,[1]* Koichiro Aya,[1] Ko Hirano,[1] Sayaka Takehara,[1] Eriko Koketsu,[1] Reynante Lacsamana Ordonio,[1] Seung-Hyun Park,[2] Masatoshi Nakajima,[2] Miyako Ueguchi-Tanaka,[1]† Makoto Matsuoka[1]†

Some ferns possess the ability to control their sex ratio to maintain genetic variation in their colony with the aid of antheridiogen pheromones, antheridium (male organ)–inducing compounds that are related to gibberellin. We determined that ferns have evolved an antheridiogen-mediated communication system to produce males by modifying the gibberellin biosynthetic pathway, which is split between two individuals of different developmental stages in the colony. Antheridiogen acts as a bridge between them because it is more readily taken up by prothalli than bioactive gibberellin. The pathway initiates in early-maturing prothalli (gametophytes) within a colony, which produce antheridiogens and secrete them into the environment. After the secreted antheridiogen is absorbed by neighboring late-maturing prothalli, it is modified in to bioactive gibberellin to trigger male organ formation.

Genetic diversity affords a competitive advantage to a particular species. Homosporous ferns have evolved a mechanism to favor cross-fertilization by controlling the sex ratio among individuals or prothalli within the population with the aid of antheridiogens. Antheridiogens are pheromones released in the aqueous environment by early-maturing fern prothalli in a colony, and they cause neighboring late-maturing prothalli in the colony to

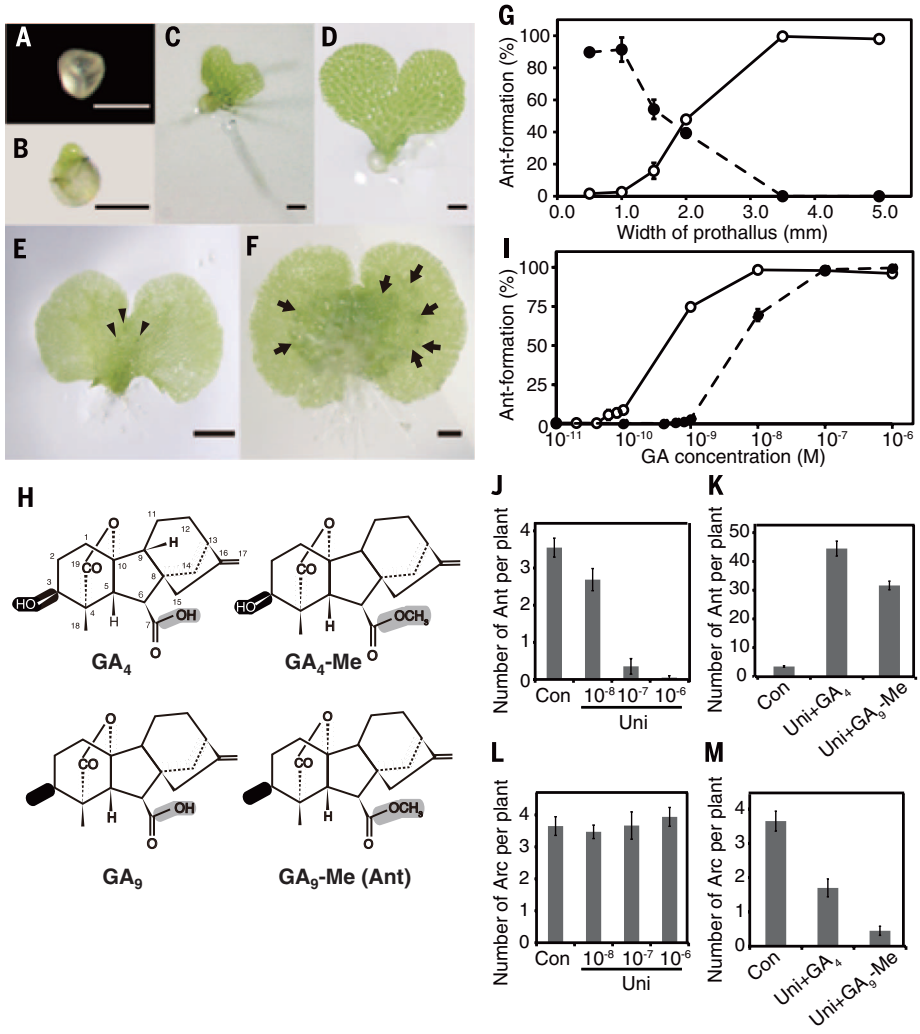

Fig. 1. Antheridiogen production, sensitivity to antheridiogen, effect of GA_4 and GA_9-Me on antheridial formation, and structures of antheridiogen-related compounds used in this study. (**A** to **F**) Prothallus of *L. japonicum* at 0 days after germination (A), 6 days (B), 13 days (~0.5 mm in size) (C), 15 days (~1.0 mm) (D), 19 days (~2.0 mm) (E), and 22 days (~5.0 mm) (F). Arrowheads, archegonia; arrows, antheridia. Scale bars, 0.1 mm [(A) to (D)], 0.5 mm [(E) and (F)]. (**G**) Antheridiogen secretion and sensitivity of prothalli during development. Solid line, secreted antheridiogen level; dashed line, sensitivity to antheridiogens; $n = 8$. (**H**) Chemical structure of antheridiogen-related compounds used in this study. Black shade, presence or absence of OH at C3; gray shade, presence or absence of methyl-esterified group at C6. (**I**) Dose dependence of GA_4 and GA_9-Me action on antheridial (Ant) formation. Solid line, GA_9-Me; Dashed line, GA_4. (**J** and **K**) Effect of Uni (10^{-8}, 10^{-7}, and 10^{-6} M), Uni (10^{-6} M) + GA_4 (10^{-7} M), and Uni (10^{-6} M) + GA_9-Me (10^{-7} M) on antheridial formation; $n = 8$. (**L** and **M**) Effect of Uni, Uni (10^{-6} M) + GA_4 (10^{-7} M), and Uni (10^{-6} M) + GA_9-Me (10^{-7} M) on archegonial (Arc) formation; $n = 8$. Con denotes control (no chemical treatment).

develop male organs (antheridia), thus promoting outcrossing in the colony (*1*–*3*). We first, by bioassay, measured the amount of antheridiogens secreted by prothalli of *Lygodium japonicum* at different developmental stages (Fig. 1, A to F). Prothalli were grown on media to a specified size (0.5 to 5 mm) and then replaced with protonemata (structure prior to prothallus stage). The amount of antheridiogens secreted by the prothalli was estimated by measuring antheridial formation of protonemata (solid line in Fig. 1G). Prothalli larger than 1.5 mm in size gradually started to secrete antheridiogens, and prothalli larger than 3.5 mm secreted enough antheridiogens for protonemata to form 100% antheridia. We also determined the sensitivity of prothalli to antheridiogens by growing prothalli on media under excess amounts of antheridiogens and examined them for antheridial formation (dashed line in Fig. 1G). Young prothalli (≤1 mm) had the greatest tendency to form antheridia, whereas prothalli larger than 3.5 mm were completely insensitive to antheridiogens. These results demonstrate that there is an antiparallel relationship between synthesis/secretion and perception of antheridiogens in adult and young prothalli, respectively.

Antheridiogens in *L. japonicum* (*4*, *5*) share a common *ent*-gibberellane skeleton with gibberellin A_4 (GA_4), the most bioactive gibberellin (GA) in seed plants (Fig. 1H). Although GA_4 is capable of inducing antheridium formation (Fig. 1I), all known natural antheridiogens lack the OH group at C3 that is essential for active GAs. In addition, antheridiogens also possess a methyl-esterified carboxyl group at C6 (Fig. 1H), which hinders GA activity (*6*). In this study, we used GA_9 methyl ester (GA_9-Me) as an antheridiogen, which has 10 times the antheridium-inducing ability of GA_4 (solid line in Fig. 1I). When a GA synthesis inhibitor, uniconazole (Uni) (*7*), was applied, it severely inhibited antheridial formation in prothalli, but not archegonial (female organ) formation (Fig. 1, J and L), whereas cotreatment with uniconazole and 10^{-7} M GA_9-Me or GA_4 promoted antheridial formation but suppressed archegonial formation (Fig. 1, K and M), indicating a dual role of antheridiogens and GA_4 in controlling the sexes (*8*).

The above and previous observations (*5*) indicate that antheridiogens in *L. japonicum* might be synthesized, at least in part, through the GA biosynthetic pathway. Thus, we attempted to isolate *L. japonicum* genes encoding GA synthesis–related enzymes (*9*), specifically *ent*-copalyl diphosphate synthase (CPS), *ent*-kaurene synthase (KS), *ent*-kaurene oxidase (KO), *ent*-kaurenoic acid oxidase (KAO), GA 20-oxidase (GA20ox), and GA 3-oxidase (GA3ox), along with the key components for GA perception (*10*), including the GID1 GA receptor, DELLA protein (a suppressor of GA signaling), and GID2/SLY1 (an F-box protein in GA signaling) (fig. S1). As *L. japonicum* has 58 chromosomes per haploid with more than 1.1×10^9 base pairs (*11*, *12*), we took the RNA sequence strategy for gene isolation. Finally, we cloned and validated the above GA-related genes, and designated them as *Lj_CPS/KS*, *Lj_KO*, *Lj_KAO*, *Lj_GA20ox*, *Lj_GA3ox1* and *2*, *Lj_GID1-1*, *-2*, and *-3*, *Lj_DELLA1* and *2*, and *Lj_GID2* (fig. S2 to S7, table S1, and table S2). Among the genes with two orthologs identified in *L. japonicum*, *Lj_GA3ox1*, *Lj_GID1-1* (*Lj_GID1-3* does not contain the GA receptor activity; see below), and *Lj_DELLA1* were expressed at higher levels in prothalli (fig. S8).

To investigate the molecular events caused by GA_9-Me and GA_4, we first examined their effects

[1]Bioscience and Biotechnology Center, Nagoya University, Nagoya 464-8601, Japan. [2]Department of Applied Biological Chemistry, University of Tokyo, Tokyo 113-8657, Japan.
*These authors contributed equally to this work. †**Corresponding author. E-mail: mueguchi@nuagr1.agr.nagoya-u.ac.jp (M.U.-T.); makoto@nuagr1.agr.nagoya-u.ac.jp (M.M.)**

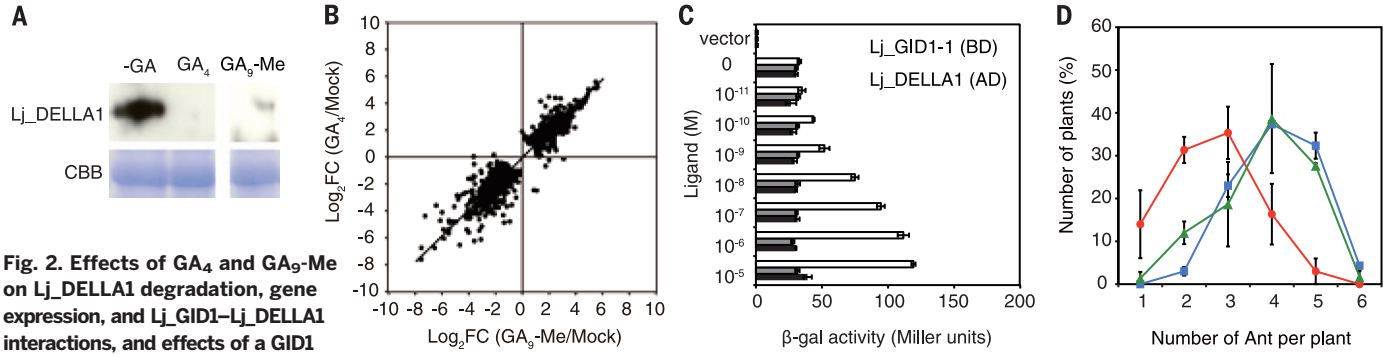

Fig. 2. Effects of GA_4 and GA_9-Me on Lj_DELLA1 degradation, gene expression, and Lj_GID1–Lj_DELLA1 interactions, and effects of a GID1 inhibitor on antheridial formation. (**A**) Degradation of Lj_DELLA1 protein in prothalli after GA_4 and GA_9-Me treatments. (**B**) Comparison of gene expression patterns in prothalli treated with 10^{-6} M GA_4 or 10^{-7} M GA_9-Me for 1 hour. Black line represents the regression line calculated by the least-squares method ($y = 0.9686x - 0.0434$, $R^2 = 0.91081$). (**C**) Yeast two-hybrid assay for the interaction of Lj_GID1-1 as prey and Lj_DELLA1 as bait under various concentrations of GA_4 (white bars), GA_9-Me (gray bars), and GA_4-Me (black bars). The β-gal activity was determined through a liquid assay with yeast (Y187) transformants ($n = 3$). (**D**) Inhibitory effect of TSPC on antheridial formation. Treatment with 10^{-9} M GA_9-Me induced 2 to 6 antheridia per protonema (blue line), whereas co-treatment with 5×10^{-7} M TSPC decreased antheridial formation (red line); 10^{-5} M GA_4 completely counteracted the inhibitory effect of TSPC (green line).

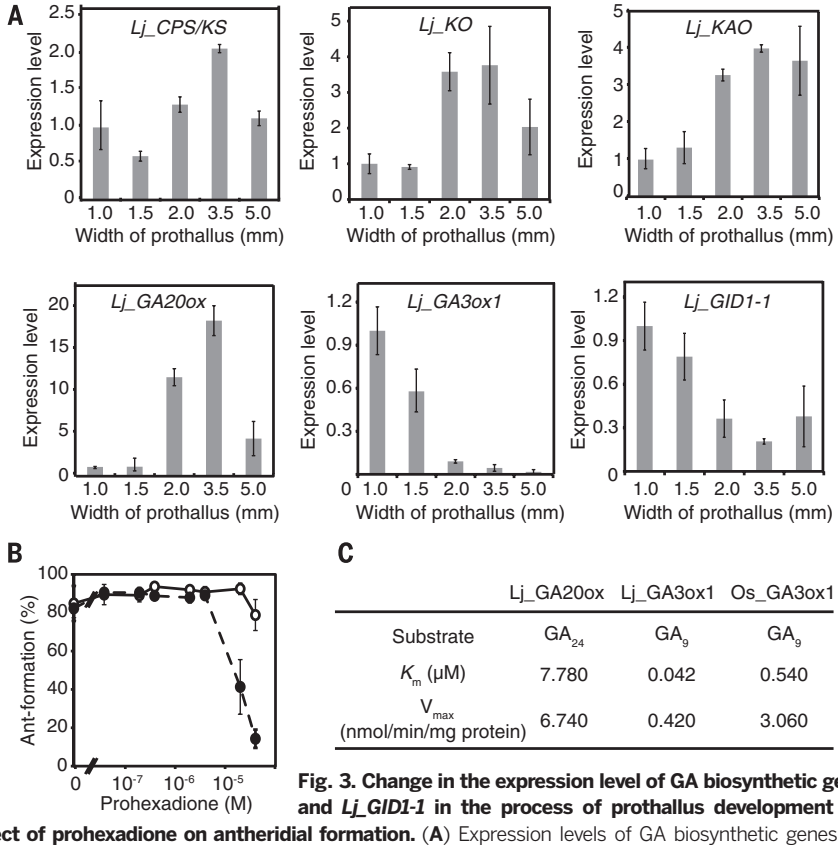

C

	Lj_GA20ox	Lj_GA3ox1	Os_GA3ox1
Substrate	GA_{24}	GA_9	GA_9
K_m (μM)	7.780	0.042	0.540
V_{max} (nmol/min/mg protein)	6.740	0.420	3.060

Fig. 3. Change in the expression level of GA biosynthetic genes and *Lj_GID1-1* in the process of prothallus development and effect of prohexadione on antheridial formation. (**A**) Expression levels of GA biosynthetic genes and *Lj_GID1-1* in prothalli of various sizes. (**B**) Inhibitory effect of prohexadione on antheridial formation in the presence of GA_4 and GA_9-Me. Solid line, 10^{-8} M GA_4; dashed line, 10^{-9} M GA_9-Me. (**C**) Comparisons of K_m and V_{max} (maximum substrate concentration) among Lj_GA20ox, Lj_GA3ox1, and Os_GA3ox1.

on the degradation of the GA signaling repressor DELLA, which is the primary event of GA response (*13*, *14*). By immunoblotting proteins extracted from young prothalli treated with either GA_9-Me or GA_4 for 1 hour, we detected the degradation of Lj_DELLA1 in both treatments (Fig. 2A). Further, we compared the effects of GA_9-Me and GA_4 on gene expression by transcriptome analysis (Fig. 2B). Among the 2213 unigenes differentially expressed between GA_9-Me and the mock treatment at a significant level ($P < 0.001$, false discovery rate <0.01, factor of ≥2 difference) (table S3), almost all were regulated in a similar manner by GA_4, with high correlations. These results indicate that GA_9-Me, like GA_4, elicits GA signaling via the GID1-DELLA system.

To examine whether GA_9-Me is directly perceived by the GID1-DELLA system, we performed a yeast two-hybrid assay to detect the interaction of Lj_GID1-1 and Lj_DELLA1 (Fig. 2C). GA_4 caused a dose-dependent interaction, which was detected even at 10^{-10} M of GA_4, a concentration lower than that required for GID1-DELLA interactions in seed plants by one to two orders of magnitude (*15*, *16*). This indicates that Lj_GID1-1 is especially adapted for detecting and interacting with minute amounts of GA_4. On the other hand, neither GA_9-Me nor GA_4-Me showed any noticeable interactions even at higher concentrations (Fig. 2C). Similar interaction profiles were also seen in other Lj_GID1–Lj_DELLA combinations, with the exception of Lj_GID1-3, which did not interact with any Lj_DELLAs under any conditions (fig. S9). This indicates that GA_9-Me itself cannot bind to Lj_GID1s or elicit GA signaling. We also examined the involvement of GID1 in antheridial formation with the use of a GID1 inhibitor, 3-(2-thienylsulfonyl) pyrazine-2-carbonitrile (TSPC), which is assumed to competitively inhibit GA binding to GID1 (*17*). Treatment with 5×10^{-7} M TSPC inhibited antheridial formation elicited by 10^{-9} M GA_9-Me, whereas cotreatment with 10^{-5} M GA_4 almost rescued the inhibitory effect of TSPC (Fig. 2D). This suggests that antheridial formation by GA_9-Me is mediated by GID1.

Next, we examined the expression pattern of GA biosynthetic genes during prothallus development by quantitative reverse transcription polymerase chain reaction (qRT-PCR) (Fig. 3A). Adult prothalli (3.5 mm) preferentially expressed *Lj_CPS/KS*, *Lj_KO*, *Lj_KAO*, and especially *Lj_GA20ox*, which was expressed at a level 10 to 20 times that in young prothalli. On the other hand, young prothalli (1.0 mm) expressed *Lj_GA3ox1* at a level 10 to 20 times that in adult prothalli, and a similar expression pattern was also observed for *Lj_GID1-1*. Such an antiparallel expression pattern between *Lj_GA20ox* and *Lj_GA3ox1* is very similar to the pattern of antheridiogen synthesis/secretion and antheridiogen sensitivity of prothalli (Fig. 1G). Next, to examine the dependence of antheridial formation on the C3 hydroxylation of antheridiogens by GA3ox, we examined the effect of a GA3ox inhibitor, prohexadione (*18*), on antheridial formation in the presence of 10^{-8} M GA_4 and

10^{-9} M GA_9-Me, which both induce 75% antheridial formation (Fig. 1I). When cotreated with GA_9-Me (which lacks the OH group at C3), prohexadione started to inhibit antheridial formation around 4×10^{-6} M and reduced it to ~10% at 4×10^{-5} M (Fig. 3B). In contrast, in the presence of GA_4 (possessing the OH group at C3), prohexadione did not inhibit at 2×10^{-5} M and caused a decline only at ~4×10^{-5} M. These results demonstrate that the C3 hydroxylation of antheridiogens is essential for antheridial formation, and therefore that antheridiogens are precursors of a compound that induces antheridial formation. This corresponds with the observation that the expression pattern of *Lj_GA3ox1* is similar to that of antheridiogen sensitivity (Fig. 1G). We then compared the enzymatic property of Lj_GA3ox1 produced in *Escherichia coli* to that of rice GA3ox (Os_GA3ox1) (Fig. 3C and fig. S10). The K_m (Michaelis constant) value of Lj_GA3ox1 to the substrate, GA_9, was 42 nM, which was not only lower than that of Os_GA3ox1 (K_m = 540 nM) but also lower than those of GA3oxs from other seed plants, such as *Arabidopsis* At_GA3ox1 (K_m = 1 μM) (*19*) and wheat GA3ox (K_m = 1 μM) (*20*). In contrast, relative to Lj_GA3ox1, the affinity of Lj_GA20ox for its substrate, GA_{24}, was lower by more than two orders of magnitude (K_m = 7.78 μM). These observations demonstrate that Lj_GA3ox1 has an unusual enzymatic property adapted for low substrate concentrations.

If antheridiogens are precursors of an antheridium-inducing compound, GA_4, why do ferns not directly use GA_4 as an antheridiogen? It may be because antheridiogens must be specially adapted for transport across the aqueous environment and have an affinity to, and interaction with, neighboring prothalli. To clarify such possibilities, we incubated young prothalli in a solution containing GA_9, GA_9-Me, GA_4, and GA_4-Me (2 μg/ml each). After removing the prothalli, the remaining GAs in the solution were measured by gas chromatography–mass spectrometry (GC-MS). We observed that GA_9-Me, and to a lesser extent GA_9, were preferentially taken up by prothalli (Fig. 4A). In another experiment, young prothalli preferentially and rapidly absorbed radioactive [^{14}C]GA_9-Me in a concentration-dependent manner, whereas the amount of [^{3}H]GA_4 absorbed was much less and did not reach the level of [^{14}C]GA_9-Me even after a considerable incubation period (Fig. 4B). Both methyl esterification of the carboxyl group and the absence of the hydroxyl group at C3 should result in the hydrophobicity of antheridiogens (Fig. 1H) and hence a higher affinity and faster interaction with hydrophobic materials, such as prothalli in aqueous conditions. Finally, we directly assayed the conversion of GA_9-Me into GA_9 by prothalli (Fig. 4C). The endogenous amount of GA_9 in young (1.0 mm) and adult (5.0 mm) prothalli was similar. Although the GA_9 level in young prothalli increased by a factor of ~3.5 after incubation with GA_9-Me, such an increase did not occur in adult prothalli. This indicates that incorporation and conversion of GA_9-Me into GA_9 occurs in young prothalli but not in adults.

We propose a model for the antheridiogen system that involves a split GA biosynthetic pathway for interindividual communication to regulate the sex ratio in a colony (Fig. 4D). First, early-maturing prothalli in a colony express GA-biosynthetic genes, except *GA3ox*, thus producing a GA_9 intermediate that lacks the OH group at C3. To be effectively transmitted to the surrounding prothalli, GA_9 is modified into an antheridiogen by methyl esterification of its C6 carboxyl group before being secreted to the outside environment. In this transmission process, there is the possible involvement of transporter(s) specific for antheridiogen. Second, antheridiogens are incorporated into neighboring late-maturing prothalli in a colony, which highly express *GA3ox*. Imported antheridiogen is first hydrolyzed to release the methyl group at C6—probably by a methyl esterase, because Lj_GA3ox1 cannot metabolize GA_9-Me into GA_4-Me (fig. S11)—and is then metabolized by GA3ox into GA_4. Finally, GA_4 is perceived by the GID1-DELLA system with the aid of GID2. Activation of the GA signaling pathway causes specific expression to induce and suppress antheridial and archegonial formation, respectively, to maintain an appropriate population of outcrossing male and female prothalli in the colony. To establish this system, GA3ox and GID1, two proteins required for antheridiogen perception, have evolved in *L. japonicum*. Relative to the GID1s of seed plants, the affinity of Lj_GID1-1 for GA_4 was higher by one to two orders of magnitude (Fig. 2C), and Lj_GA3ox1 showed a much higher affinity for its substrate relative to other GA3oxs from seed plants (Fig. 3C). These findings indicate that the two proteins have become attuned to very low concentrations of their substrates within young prothalli.

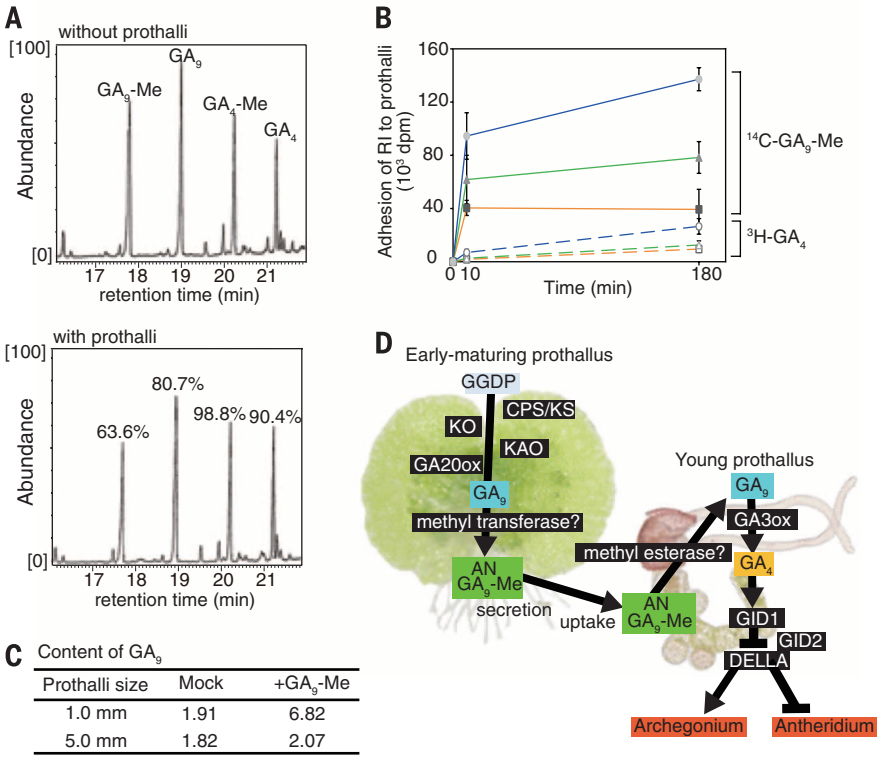

Fig. 4. Uptake of GA_9-Me by prothalli and molecular model of antheridial formation by antheridiogen in *L. japonicum*. (**A**) Uptake of various GAs from solution by young prothalli. Top panel, without prothalli. Bottom panel, with prothalli; percentages of remaining GAs in solution relative to the top panel are shown. (**B**) Accumulation of radioactive GAs in prothalli at different concentrations with respect to incubation time. Dashed lines, [^{3}H]GA_4; solid lines, [^{14}C]GA_9-Me; orange, 5.9 μM; green, 11.8 μM; blue, 23.6 μM. (**C**) GA_9 content (ng/g fresh weight) of young (1.0 mm) and adult (5.0 mm) prothalli with or without incubation with 0.6 mM GA_9-Me for 3 hours. (**D**) Proposed model for fern antheridiogen system.

REFERENCES AND NOTES

1. U. Näf, in *The Experimental Biology of Ferns: Antheridiogens and Antheridial Development*, A. F. Dyer, Ed. (Academic Press, New York, 1979), pp. 436–470.
2. J. J. Schneller, *Biology and Evolution of Ferns and Lycophytes: Antheridiogens* (Cambridge Univ. Press, Cambridge, 2008), pp. 134–158.
3. B. Voeller, E. Weinberg, in *Current Topics in Plant Science: Evolutionary and Physiological Aspects of Antheridium Induction in Ferns*, J. Gunkel, Ed. (Academic Press, New York, 1969), pp. 77–93.
4. H. Yamane, N. Takahashi, K. Takeno, M. Furuya, *Planta* **147**, 251–256 (1979).
5. H. Yamane, *Int. Rev. Cytol.* **184**, 1–32 (1998).
6. P. Hedden, *Nature* **456**, 455–456 (2008).
7. K. Izumi *et al.*, *Plant Cell Physiol.* **26**, 821–827 (1985).
8. K. Takeno, M. Furuya, *Bot. Mag.* **93**, 67–76 (1980).
9. S. Yamaguchi, *Annu. Rev. Plant Biol.* **59**, 225–251 (2008).
10. M. Ueguchi-Tanaka, M. Nakajima, A. Motoyuki, M. Matsuoka, *Annu. Rev. Plant Biol.* **58**, 183–198 (2007).
11. B. Y. S. K. Roy, I. Manton, *New Phytol.* **64**, 286–292 (1965).
12. L. Hanson, I. J. Leitch, *Bot. J. Linn. Soc.* **140**, 169–173 (2002).

13. A. Dill, H. S. Jung, T. P. Sun, *Proc. Natl. Acad. Sci. U.S.A.* **98**, 14162–14167 (2001).
14. H. Itoh, M. Ueguchi-Tanaka, Y. Sato, M. Ashikari, M. Matsuoka, *Plant Cell* **14**, 57–70 (2002).
15. M. Nakajima *et al.*, *Plant J.* **46**, 880–889 (2006).
16. Y. Yamamoto *et al.*, *Plant Cell* **22**, 3589–3602 (2010).
17. J. M. Yoon *et al.*, *Bioorg. Med. Chem. Lett.* **23**, 1096–1098 (2013).
18. I. Nakayama *et al.*, *Plant Cell Physiol.* **31**, 1183–1190 (1990).
19. J. Williams, A. L. Phillips, P. Gaskin, P. Hedden, *Plant Physiol.* **117**, 559–563 (1998).
20. N. E. J. Appleford *et al.*, *Planta* **223**, 568–582 (2006).

ACKNOWLEDGMENTS

We thank M. Kawamura and W. Takase (Nagoya University) for technical assistance and H. Yamane (Teikyo University), M. Hasebe (National Institute for Basic Biology), S. Ooe (Osaka Prefectural Education Center), and T. Yoshimura (Kumiai Chemical Industry Co., Ltd.) for helpful discussions. Supported by Grant-in-Aid for Scientific Research on Innovative Areas no. 23113005 (M.M. and M.N.) and by JSPS through the Funding Program for Next Generation World-Leading Researchers (M.U.-T.). Additional data are in the supplement. DNA Data Bank of Japan (DDBJ) accession numbers: *Lj_CPS/KS*, AB915786; *Lj_KO*, AB915787; *Lj_KAO*, AB915788; *Lj_GA20ox*, AB915789; *Lj_GA3ox1*, AB915790; *Lj_GA3ox2*, AB915791; *Lj_GID1-1*, AB915792; *Lj_GID1-2*, AB915793; *Lj_GID1-3*, AB915794; *Lj_DELLA1*, AB915795; *Lj_DELLA2*, AB915796; *Lj_GID2*, AB915797.

SUPPLEMENTARY MATERIALS

www.sciencemag.org/content/346/6208/469/suppl/DC1
Materials and Methods
Figs. S1 to S11
Tables S1 to S4
References (*21*–*28*)

12 August 2014; accepted 5 September 2014
10.1126/science.1259923

VIRAL CELL BIOLOGY

Influenza A virus uses the aggresome processing machinery for host cell entry

Indranil Banerjee,[1]*† Yasuyuki Miyake,[2] Samuel Philip Nobs,[3] Christoph Schneider,[3] Peter Horvath,[4] Manfred Kopf,[3] Patrick Matthias,[2,5] Ari Helenius,[1]‡ Yohei Yamauchi[1]‡

During cell entry, capsids of incoming influenza A viruses (IAVs) must be uncoated before viral ribonucleoproteins (vRNPs) can enter the nucleus for replication. After hemagglutinin-mediated membrane fusion in late endocytic vacuoles, the vRNPs and the matrix proteins dissociate from each other and disperse within the cytosol. Here, we found that for capsid disassembly, IAV takes advantage of the host cell's aggresome formation and disassembly machinery. The capsids mimicked misfolded protein aggregates by carrying unanchored ubiquitin chains that activated a histone deacetylase 6 (HDAC6)–dependent pathway. The ubiquitin-binding domain was essential for recruitment of HDAC6 to viral fusion sites and for efficient uncoating and infection. That other components of the aggresome processing machinery, including dynein, dynactin, and myosin II, were also required suggested that physical forces generated by microtubule- and actin-associated motors are essential for IAV entry.

Influenza A virus (IAV) is an enveloped virus of great medical impact. With the risk of an influenza pandemic growing, it is increasingly important to understand virus-host interactions in detail and to develop new antiviral strategies (*1*). IAV has a single-stranded, negative-sense RNA genome divided between eight subgenomic RNA molecules. These are individually packaged into helical viral ribonucleoproteins (vRNPs) that contain a viral polymerase complex and multiple copies of the nucleoprotein, NP. In the virus, the vRNPs form a stable, capsid-like, supramacromolecular complex with the matrix protein, M1, which forms a shell around the vRNPs (*2*). During IAV entry into a host cell (Fig. 1A, top), the uncoating process is initiated in early endosomes where the mildly acidic pH triggers the opening of the M2 channel in the viral envelope leading to influx of protons and potassium ions (*3*–*5*). A conformational change occurs that renders the capsid uncoating-competent. When the pH drops further in late endosomes (LEs), the membrane fusion function of the hemagglutinin (HA) is activated, and the capsid is transferred to the cytosol (*6*, *7*). The M1 disperses, and the vRNPs are imported into the nucleus through nuclear pore complexes (*8*–*11*).

While analyzing the role of HDAC8 and HDAC3 in endosome maturation and IAV penetration (*12*), we noticed that another histone deacetylase, HDAC6, was also required for infection. A cytosolic enzyme responsible for deacetylation of tubulin and some other substrates, it also serves as a key component in ubiquitin (Ub)–dependent aggresome formation and disassembly (*13*, *14*). We found that HDAC6 depletion by RNA interference (RNAi) in A549 cells (a human bronchial epithelial cell line) reduced infection by half (fig. S1, A and H). In HDAC6 knock-out (KO) mouse embryonic fibroblasts (MEFs), infection was reduced to 30%, and viral titers to 48%, compared with wild-type (WT) MEFs (fig. S1, B, C, and H). When WT and HDAC6 KO mice (*15*) were infected intratracheally with IAV strains PR8 and X31 in HDAC6 KO mice, lung viral titers were reduced to 48% and 31%, respectively, at day 5 compared with controls (fig. S2, A and B). The antiviral immune responses were comparable when tested in PR8-infected mice (fig. S2, C to E).

When the stepwise IAV entry was analyzed in HDAC6 KO MEFs using quantitative assays (*8*), no significant difference was observed with WT MEFs in endocytic uptake, acid-induced HA conversion, and fusion (Fig. 1A and fig. S1G). However, capsid uncoating and nuclear import of vRNPs were reduced to 22 and 17%, respectively (Fig. 1A). In HDAC6-depleted A549 cells, uncoating was reduced to 21% compared with controls, with no effect on HA acidification or fusion (fig. S1, D to F). It was apparent that HDAC6 played a role in the release of viral capsids from the cytosolic surface of endosomes, the dissociation of M1 from vRNPs, and the dispersion of capsid components in the cytosol.

To confirm that the HDAC6 requirement was postfusion, we induced fusion of the virus directly with the plasma membrane (PM), a process that allows delivery of viral capsids into the cytosol without endocytosis (fig. S3A) (*6*, *7*). Although fusion efficiency was comparable, the M1 was diffusely distributed through the cytoplasm in WT MEFs but remained punctate in HDAC6 KO MEFs (fig. S3, B and C). That uncoating was reduced to 32% in the HDAC6 KO MEFs and to 47% in HDAC6-depleted A549 cells (fig. S3, D and E) compared with control cells confirmed that HDAC6 was required after fusion.

To determine which of the functions of HDAC6 were required for uncoating, we used HDAC6 KO MEFs that had been rescued either with WT HDAC6 (WT^{r}) or with HDAC6s with point mutations either in the two deacetylase domains (HD^{m}) (*16*) or in the zinc-finger domain (ZnF^{m}) (*17*, *18*). The zinc-finger ubiquitin binding domain (ZnF-UBP) is C-terminal and binds Ub. It plays a critical role in aggresome formation and disassembly (*13*, *14*) (Fig. 1B). Whereas most Ub-binding proteins interact with the hydrophobic core of Ub, the ZnF-UBP domain of HDAC6 binds to the C-terminal Gly-Gly residues (*13*, *19*). This means that HDAC6 only binds to Ub and poly-Ub chains that are not coupled to proteins. The point

[1]Institute of Biochemistry, Eidgenossische Technische Hochschule (ETH) Zurich, Switzerland. [2]Epigenetics, Friedrich Miescher Institute for Biomedical Research, Basel, Switzerland. [3]Institute of Molecular Health Sciences, ETH Zurich, Switzerland. [4]Synthetic and Systems Biology Unit, Biological Research Center, Szeged, Hungary. [5]Faculty of Sciences, University of Basel, Basel, Switzerland.
*Present address: Developmental and Molecular Pathways, Novartis Institutes for Biomedical Research, Basel, Switzerland. †Present address: Neural Circuit Laboratories, Friedrich Miescher Institute for Biomedical Research, Basel, Switzerland. **‡Corresponding author. E-mail: ari.helenius@bc.biol.ethz.ch (A.H.); yohei.yamauchi@bc.biol.ethz.ch (Y. Y.)**

Editor's Summary

Sex determination driven by community cooperation

An optimized ratio of male and females in a sexually reproducing population helps to generate the genetic diversity useful to a species in a changing world. Tanaka *et al.* studied a fern in which the sex ratio is adjusted not by individual identity, but by signaling between individual plants (see the Perspective by Sun). Early-maturing individual ferns express some of the biosynthetic genes needed to make a precursor of the plant hormone gibberellin, which they secrete into the environment. Younger ferns, which express the enzymes needed to finalize synthesis of gibberellin, take up the signal and in response develop the organs that produce male gametes.

Science, this issue p. 469; see also p. 423